

Labyrinthine pathways towards supercycle attractors in unimodal maps

Luis G. Moyano

*Departamento de Matemáticas and Grupo Interdisciplinar de Sistemas Complejos,
Universidad Carlos III de Madrid, 28911 Leganés, Madrid, Spain*

D. Silva and A. Robledo

*Instituto de Física, Universidad Nacional Autónoma de México,
Apartado postal 20-364, México 01000 D.F., México*

We uncover previously unknown properties of the family of periodic superstable cycles in unimodal maps characterized each by a Lyapunov exponent that diverges to minus infinity. Amongst the main novel properties are the following: i) The basins of attraction for the phases of the cycles develop fractal boundaries of increasing complexity as the period-doubling structure advances towards the transition to chaos. ii) The fractal boundaries, formed by the preimages of the repeller, display hierarchical structures organized according to exponential clusterings that manifest in the dynamics as sensitivity to the final state and transient chaos. iii) There is a functional composition renormalization group (RG) fixed-point map associated to the family of supercycles. iv) This map is given in closed form by the same kind of q -exponential function found for both the pitchfork and tangent bifurcation attractors. v) There is a final stage ultra-fast dynamics towards the attractor with a sensitivity to initial conditions that decreases as an exponential of an exponential of time.

Key words: supercycles, fractal boundaries, transient chaos, RG fixed-point map

PACS: 05.45.-a, 64.60.Ht, 05.45.Df, 02.60.Cb

I. INTRODUCTION

The family of superstable orbits - often called supercycles - of unimodal maps have played a prominent role in the historical uncovering of the cascade of period-doubling bifurcations that leads to the transition to chaos with the celebrated universal features displayed by the Feigenbaum attractor [1], [2], [3]. These periodic attractors are easy to find because one of its cycle positions corresponds to the maximum of the map. And then, they are convenient for basic computational purposes because trajectories originating at different positions settle very fast into the attractor for the reason that their Lyapunov exponent diverges to minus infinity. And so they offered a suitable path for the initial characterization of the period-doubling route to chaos. Oddly enough, several features associated to the dynamical evolution toward these attractors have remained unexplored. Here we provide an account of these properties, some shared by other families of periodic attractors and some specific of the supercycles. We discuss explicitly the case of a map with quadratic maximum but the results are easily extended to general nonlinearity $z > 1$. In closing we indicate the broader theoretical interest in these properties.

In order to obtain dynamical properties with previously unstated detail we determined the organization of the *entire* set of trajectories as generated by all possible initial conditions. We find that the paths taken by the full set of trajectories in their way to the supercycle attractors (or to their complementary repellers) are far from unstructured. The preimages of the attractor of period 2^N , $N = 1, 2, 3, \dots$ are distributed into different basins of attraction, one for each of the 2^N phases (positions) that compose the cycle. When $N \geq 2$ these basins

are separated by fractal boundaries whose complexity increases with increasing N . The boundaries consist of the preimages of the corresponding repeller and their positions cluster around the $2^N - 1$ repeller positions according to an exponential law. As N increases the structure of the basin boundaries becomes more involved. Namely, the boundaries for the 2^N cycle develops new features around those of the previous 2^{N-1} cycle boundaries, with the outcome that a hierarchical structure arises, leading to embedded clusters of clusters of boundary positions, and so forth.

The dynamics associated to families of trajectories always displays a distinctively concerted order that reflects the repeller preimage boundary structure of the basins of attraction. That is, each trajectory has an initial condition that is identified as an attractor (or repeller) preimage of a given order, and this trajectory necessarily follows the steps of other trajectories with initial conditions of lower preimage order belonging to a given chain or pathway to the attractor (or repeller). This feature gives rise to transient chaotic behavior different from that observed at the last stage of approach to the attractor. When the period 2^N of the cycle increases the dynamics becomes more involved with increasingly more complex stages that reflect the preimage hierarchical structure. As a final point, at the closing part of the last leg of the trajectories an ultra-rapid convergence to the attractor is observed, with a sensitivity to initial conditions that decreases as an exponential of an exponential of time. In relation to this we find that there is a functional composition renormalization group (RG) fixed-point map associated to the supercycle attractor, and this can be expressed in closed form by the same kind of q -exponential function found for both the pitchfork and tangent bifurcation attractors [4], [5], like that originally derived by

Hu and Rudnick for the latter case [6].

Before proceeding to give details in the following sections of the aforementioned dynamics we recall basic features of the bifurcation forks that form the period-doubling cascade sequence in unimodal maps, epitomized by the logistic map $f_\mu(x) = 1 - \mu x^2$, $-1 \leq x \leq 1$, $0 \leq \mu \leq 2$ [1], [2], [3]. The superstable periodic orbits of lengths 2^N , $N = 1, 2, 3, \dots$, are located along the bifurcation forks, i.e. the control parameter value $\mu = \bar{\mu}_N < \mu_\infty$ for the superstable 2^N -attractor is that for which the orbit of period 2^N contains the point $x = 0$, where $\mu_\infty = 1.401155189\dots$ is the value of μ at the period-doubling accumulation point. The positions (or phases) of the 2^N -attractor are given by $x_m = f_{\bar{\mu}_N}^{(m)}(0)$, $m = 1, 2, \dots, 2^N$. Notice that infinitely many other sequences of superstable attractors appear at the period-doubling cascades within the windows of periodic attractors for values of $\mu > \mu_\infty$. Associated to the 2^N -attractor at $\mu = \bar{\mu}_N$ there is a $(2^N - 1)$ -repellor consisting of $2^N - 1$ positions y_m , $m = 1, 2, \dots, 2^N - 1$. These positions are the unstable solutions, $\left| df_{\bar{\mu}_N}^{(2^n-1)}(y)/dy \right| < 1$, of $y = f_{\bar{\mu}_N}^{(2^n-1)}(y)$, $n = 1, 2, \dots, N$. The first, $n = 1$, originates at the initial period-doubling bifurcation, the next two, $n = 2$, start at the second bifurcation, and so on, with the last group of 2^{N-1} , $n = N$, stemming from the $N - 1$ bifurcation. See Fig. 1. We find it useful to order the repellor positions, or simply, repellers, present at $\mu = \bar{\mu}_N$, according to a hierarchy or tree, the ‘oldest’ with $n = 1$ up to the most recent ones with $n = N$. The repellers’ order is given by the value of n . Finally, we define the preimage $x^{(k)}$ of order k of position x to satisfy $x = h^{(k)}(x^{(k)})$ where $h^{(k)}(x)$ is the k -th composition of the map $h(x) \equiv f_{\bar{\mu}_N}^{(2^N-1)}(x)$. We have omitted reference to the 2^N -cycle in $x^{(k)}$ to simplify the notation.

II. PREIMAGE STRUCTURE OF SUPERCYCLE ATTRACTORS

The core source of our description of the dynamics towards the supercycle attractors is a measure of the relative ‘time of flight’ $t_f(x_0)$ for a trajectory with initial condition x_0 to reach the attractor. The function $t_f(x_0)$ is obtained for an ensemble representative of *all* initial conditions $-1 \leq x_0 \leq 1$. This comprehensive information is determined through the numerical realization of every trajectory, up to a small cutoff $\varepsilon > 0$ at its final stage. The cutoff ε regards a position $x_f \leq x_m \pm \varepsilon$ to be effectively the attractor phase x_m . This, of course, introduces an approximation to the real time of flight, that can be arbitrarily large for those x_0 close to a repellor position y_m or close to any of its infinitely many preimages, $x_m^{(k)}$, $k = 1, 2, \dots, N \geq 2$. In such cases the finite time $t_f(x_0; \varepsilon)$ can be seen to diverge $t_f \rightarrow \infty$ as $x_0 \rightarrow y_m$ and $\varepsilon \rightarrow 0$. As a simple illustration, in Fig. 2 we show the time of flight $t_f(x_0)$ for the period

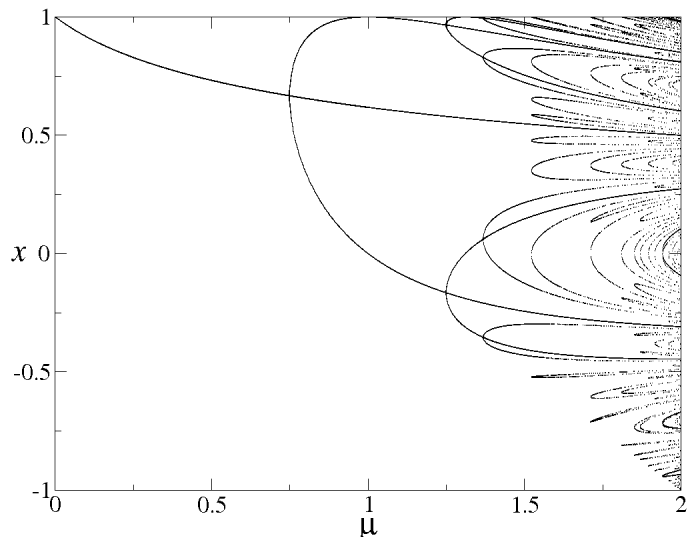


FIG. 1: Solutions of $x = f_\mu^{(2^N)}(x)$, $N = 0, 1, 2, \dots$, where f_μ is the logistic map, as a function of the control parameter μ . The attractors (stable solutions) become unstable at each bifurcation, turning into repellers. When for a given value of μ the attractor has 2^N positions there are $2^N - 1$ repellor positions.

2 supercycle at $\mu = \bar{\mu}_1$ with $\varepsilon = 10^{-9}$ together with the twice-composed map $f_{\bar{\mu}_1}^{(2)}(x)$ and a few representative trajectories. We observe two peaks in $t_f(x_0; \varepsilon)$ at $y_1 = (-1 + \sqrt{1 + 4\bar{\mu}_1})/2\bar{\mu}_1 \simeq 0.618034\dots$, the fixed-point repellor and at its (only) preimage $x_1^{(1)} = -y_1$, where $y_1 = f_{\bar{\mu}_1}^{(2)}(x_1^{(1)})$. Clearly, there are two basins of attraction each for the two positions or phases, $x_1 = 0$ and $x_2 = 1$, of the attractor. For the former it is the interval $x_1^{(1)} < x_0 < y_1$, whereas for the second one consists of the intervals $-1 \leq x_0 < x_1^{(1)}$ and $y_1 < x_0 \leq 1$. The multiple-step structure of $t_f(x_0)$, of four time units each step, reflects the occurrence of intervals of initial conditions with common attractor phase preimage order k .

For the next supercycle - period 4 - the preimage structure turns out to be a good deal more involved than the straightforward structure for $\bar{\mu}_1$. In Fig. 3 we show the times of flight $t_f(x_0)$ for the $N = 2$ supercycle at $\mu = \bar{\mu}_2$ with $\varepsilon = 10^{-9}$, the map $f_{\bar{\mu}_2}^{(4)}(x)$ is superposed as a reference to indicate the four phases of the attractor (at $x_1 = 0$, $x_2 = 1$, $x_3 \simeq -0.3107\dots$, and $x_4 \simeq 0.8734\dots$) and the three repellor positions (at $y_1 \simeq 0.5716635\dots$, $y_2 \simeq 0.952771\dots$, and $y_3 \simeq -0.189822\dots$). In Fig. 3 there are also shown four trajectories each of which terminates at a different attractor phase. We observe a proliferation of peaks and valleys in $t_f(x_0)$, actually, an infinite number of them, that cluster around the repellor at $y_1 \simeq 0.5716635\dots$ and also at its preimage at $x_1^{(1)} = -y_1$ (these are the positions at $\mu = \bar{\mu}_2$ of the ‘old’ repellor and its preimage in the previous $N = 1$ case). Notice

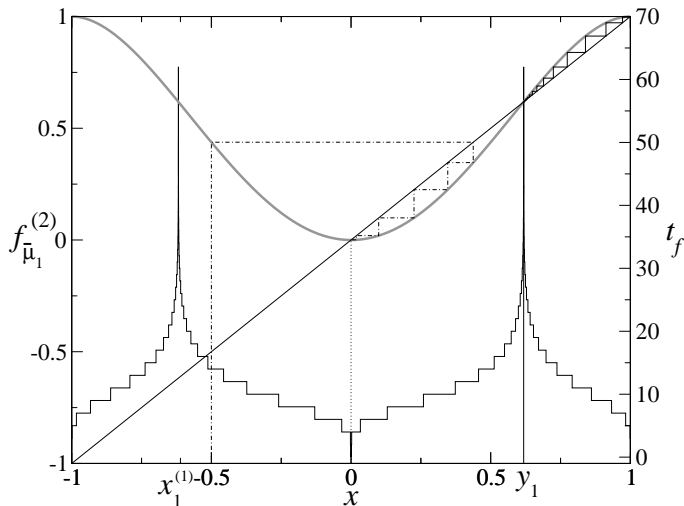


FIG. 2: Left axis: The twice iterated map $f_{\bar{\mu}_1}^{(2)}(x)$, $\bar{\mu}_1 = 1$ (in grey line). Right axis: Time of flight $t_f(x)$, the number of iterations necessary for a trajectory with initial condition at x to reach an attractor position. The values of x near the high spikes correspond to initial conditions very close to the repeller and its preimage. We present three example trajectories (and the $y = x$ line as an aid to visualize them): The dotted line shows a trajectory that starts at the attractor position $x = 0$ and remains there. The solid line is a trajectory starting near the repeller at y_1 , and after a large number of iterations reaches the attractor position $x = 1$. Finally, the dash-dotted line is an orbit starting at $x = 0.5$ that in just a few iterations reaches $x = 0$.

that the steps in the valleys of $t_f(x_0)$ are now eight time units each. The nature of the clustering of peaks (repellor phase preimages) and the bases of the valleys (attractor phase preimages) is revealed in Fig. 4 where we plot t_f in a logarithmic scale for the variables $\pm(x - y_1)$. There is an exponential clustering of the preimage structure around both the old repeller and its preimage. This scaling property is corroborated in Fig. 5 from where we obtain $x - y_1 \simeq 7.5 \times 10^{-5} \exp(0.80 l)$, where $l = 1, 2, 3, \dots$ is a label for consecutive repellor preimages.

A comparable leap in the complexity of the preimage structure is observed for the following - period 8 - supercycle. In Fig. 6 we show $t_f(x_0)$ for the $N = 3$ supercycle at $\mu = \bar{\mu}_3$ with $\varepsilon = 10^{-9}$, together with the map $f_{\bar{\mu}_2}^{(8)}(x)$ placed as reference to facilitate the identification of the locations of the eight phases of the attractor, x_1 to x_8 , and the seven repellor positions, y_1 to y_7 . Besides a huge proliferation of peaks and valleys in $t_f(x_0)$, we observe now the development of clusters of clusters of peaks centered around the repeller at $y_1 \simeq 0.5626447 \dots$ and its preimage at $x_1^{(1)} = -y_1$ (these are now the positions of the original repeller and its preimage for the $N = 1$ case when $\mu = \bar{\mu}_3$). The steps in the valleys of $t_f(x_0)$ have become sixteen time units each. Similarly to the clustering of peaks (repellor phase preimages) and valleys (attractor phase preimages) for the pre-

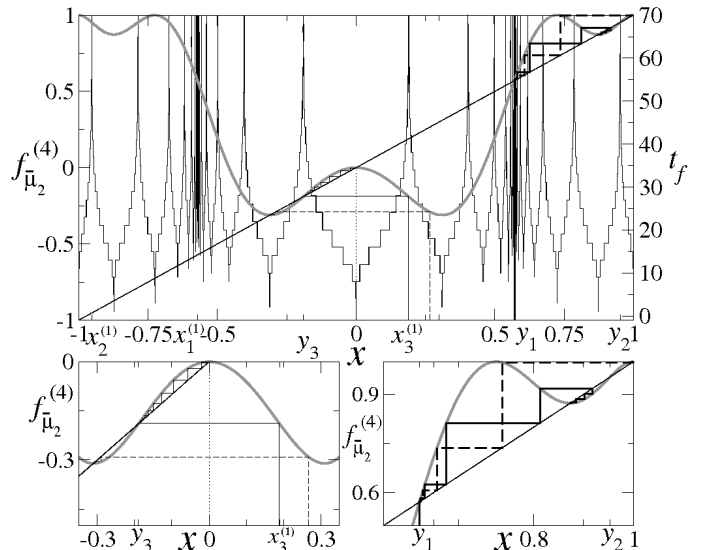


FIG. 3: Same as Fig. 2 but for $f_{\bar{\mu}_2}^{(4)}(x)$, $\bar{\mu}_2 \simeq 1.31070264$. Two orbits (in solid bold and dashed bold lines) start very near each other and by the position y_1 of the old repellor, indistinguishable at the beginning they take very different subsequent paths to reach the attractor positions at $x = 1$ and $x \simeq 0.8734$. See bottom right panel. Another two orbits (in dotted and solid lines) start at an attractor position $x = 1$ and at a repellor preimage positions, respectively. Finally, one more orbit (in dashed line) starts at an intermediate initial condition and reaches very quickly the attractor position at $x \simeq -0.310703$. See bottom left panel.

vious supercycle at $\bar{\mu}_2$, the spacing arrangement of the new clusters of clusters of peaks is determined in Fig. 7 where we plot t_f in a logarithmic scale for the variables $\pm(x - y_1)$. In parallel to the previous cycle an exponential clustering of clusters of the preimage structure is found around both the old repeller and its preimage. This scaling property is quantified in Fig. 8 from where we obtain $x - y_1 \simeq 8.8 \times 10^{-5} \exp(0.84 l)$, where $l = 1, 2, 3, \dots$ counts consecutive clusters.

An investigation of the preimage structure for the next $N = 4$ supercycle at $\mu = \bar{\mu}_4$ leads to another substantial increment in the involvedness of the structure of preimages but with such density that makes it cumbersome to describe here. Nevertheless it is clear that the main characteristic in the dynamics is the development of a hierarchical organization of the preimage structure as the period 2^N of the supercycles increases.

III. FINAL STATE SENSITIVITY AND TRANSIENT CHAOS

With the knowledge gained about the features displayed by the times of flight $t_f(x_0)$ for the first few supercycles it is possible to determine and understand how the leading properties in the dynamics of approach to these attractors arise. The information contained in $t_f(x_0)$ can

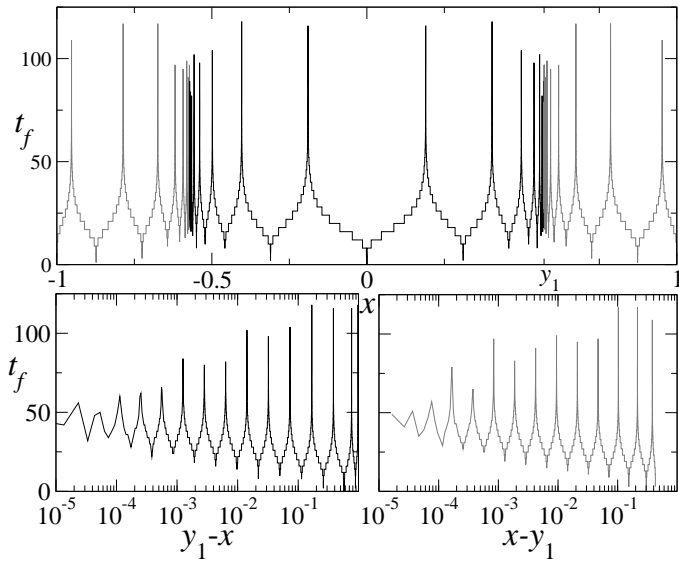


FIG. 4: Top panel: Time of flight $t_f(x)$ for $N = 2$ (as in Fig. 3), the black lines correspond to initial conditions that terminate at the attractor positions $x = 0$ and $x \simeq -0.310703$, while the grey lines to trajectories ending at $x = 1$ and $x \simeq 0.8734$. Right (left) bottom panel: Same as top panel, but plotted against the logarithm of $x - y_1$ ($y_1 - x$). It is evident that the peaks are arranged exponentially around the old repeller position y_1 , i.e., they appear equidistant in a logarithmic scale. See Fig. 5.

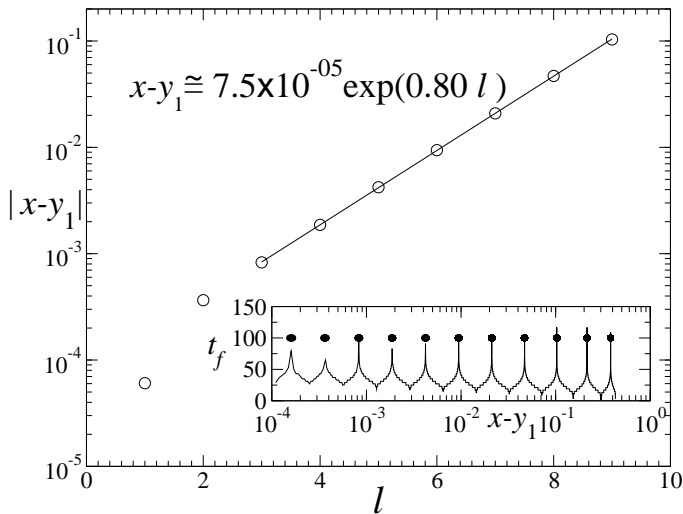


FIG. 5: Corroboration of preimage exponential clustering around the repeller position $y_1 \simeq 0.571663$ when $N = 2$ and $\bar{\mu}_2 \simeq 1.31070264$. The variable l labels consecutive equidistant peaks in the inset. The peaks correspond to preimages of the repeller. See text.

be used to demonstrate in detail how the concepts of final state sensitivity [7] - due to attractor multiplicity - and transient chaos [2] - prevalent in the presence of repellers that coexist with periodic attractors - realize in a given dynamics. Final state sensitivity is the con-

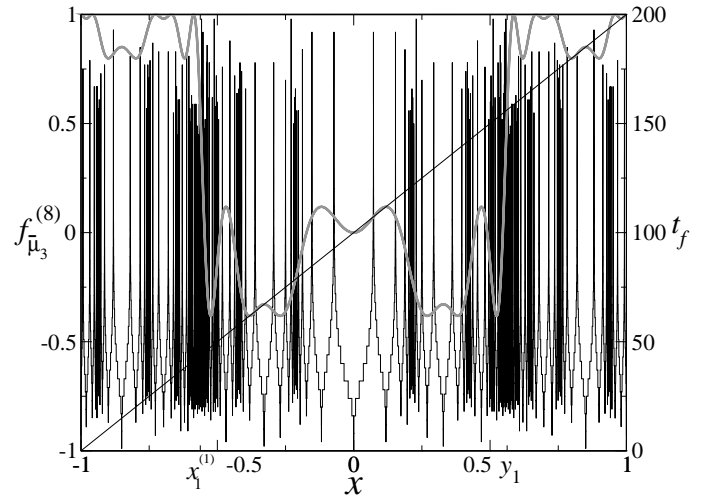


FIG. 6: Same as Fig. 3 for $f_{\bar{\mu}_3}^{(8)}(x)$, $\bar{\mu}_3 \simeq 1.38154748$. Here $y_1 = 0.56264475$.

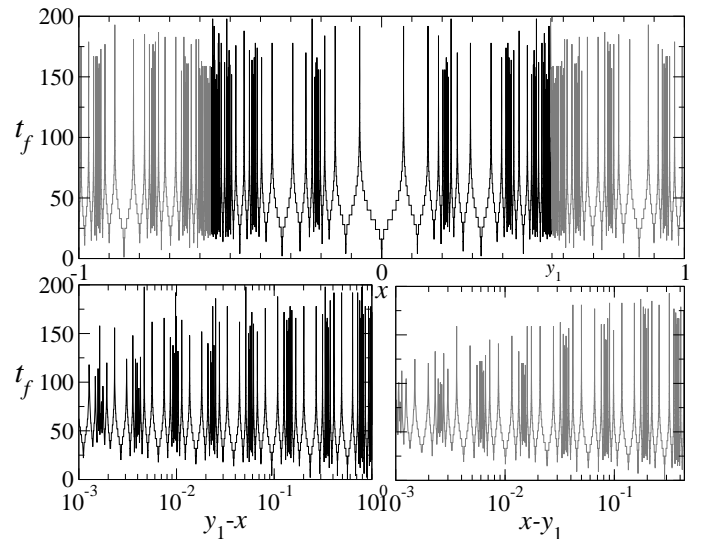


FIG. 7: Same as Fig. 4 for $N = 3$. The black lines correspond to initial conditions that terminate at any of the four attractor positions close or equal to $x = 0$, while the grey lines to trajectories ending at any of the other four attractor positions close or equal to $x = 1$. As the bottom panels show, in logarithmic scale, in this case there are (infinitely) many clusters of peaks (repeller preimages) equidistant from each other.

sequence of fractal boundaries separating coexisting attractors. In our case there is always a single attractor but its positions or phases play an equivalent role [8]. Transient chaos [2] is due to fast separation in time of nearby trajectories by the action of a repeller and results in a sensitivity to initial conditions that grows exponentially up to a crossover time after which the decay sets in. We describe below how both properties result from an extremely ordered flow of trajectories towards the attractor. This order is imprinted by the preimage structure

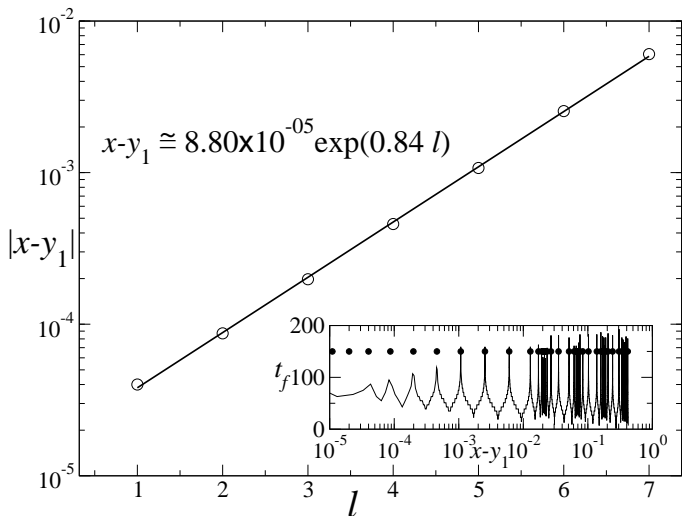
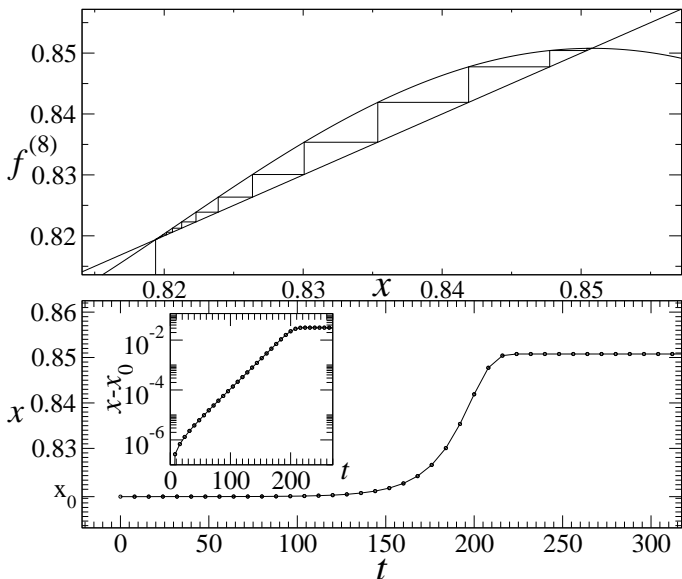
FIG. 8: Same as Fig. 5 for $N = 3$.

FIG. 9: Top panel: Detail of the map $f_{\bar{\mu}_3}^{(8)}(x)$ and a trajectory in the proximity of the attractor position located at $x \simeq 0.850780$. The trajectory originated very close to the repeller position at $x = 0.819378$. Bottom panel: The same trajectory of the eight-iterated map as a function of time t . Inset: Corroboration of the exponential nature of the trajectory after it leaves the repeller and before the final approach to the attractor position.

described in the previous section.

For the simplest supercycle at $\mu = \bar{\mu}_1$ there is trivial final state sensitivity as the boundary between the two basins of the phases, $x_1 = 0$ and $x_2 = 1$, consists only of the two positions, $y_1 \simeq 0.5716635\dots$ and $x_1^{(1)} = -y_1$. See Fig. 2. Consider the length δ of a small interval around a given value of x_0 containing either y_1 or $x_1^{(1)}$, when $\delta \rightarrow 0$ any uncertainty as to the final phase of the trajectory disappears. It is also simple to verify that when x_0 is

close to y_1 or $x_1^{(1)}$ the resulting trajectories increase their separation at initial and intermediate times displaying transient chaos in a straightforward fashion. In Fig. 9 we show the same type of transitory exponential sensitivity to initial conditions for a trajectory at $\mu = \bar{\mu}_3$ after it reaches a repeller position in the final journey towards the period 8 attractor. This behavior is common to all periodic attractors when trajectories come near a repeller at the final leg of their journey.

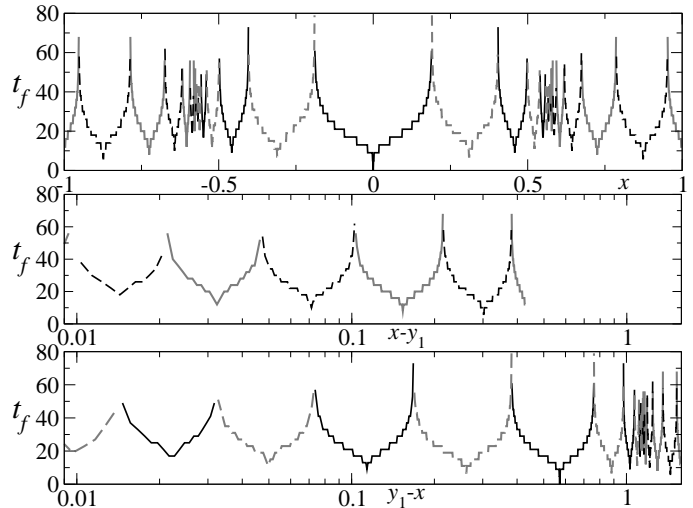


FIG. 10: Time of flight $t_f(x)$ for $N = 2$ (equivalent to Fig. 4). Different types of lines are used for different sub-basins of attraction that form the fractal boundary between the attractor positions. The black solid line corresponds to the attractor position $x = 0$, the grey solid line to $x = 1$, dashed grey line to $x \simeq -0.310703$, and dashed black line to $x \simeq 0.873470$. The sub-basins are separated in an alternated fashion by repeller preimages (peaks) and there are just two types of sub-basins depending on $|x|$ being larger or smaller than y_1 .

For $\mu = \bar{\mu}_2$ there are more remarkable properties arising from the more complex preimage structure. There is a concerted migration of initial conditions seeping through the boundaries between the four basins of attraction of the phases. These boundaries, shown in Fig. 10, form a fractal network of interlaced sub-basins separated from each other by two preimages of different repeller phases and have at their bottom a preimage of an attractor phase. Trajectories on one of these sub-basins move to the nearest sub-basin of its type (next-nearest neighbor in actual distance in Fig. 10) at each iteration of the map $f_{\bar{\mu}_2}^{(4)}$ (4 time steps for the original map $f_{\bar{\mu}_2}$). The movement is always away from the center of the cluster at the old repeller position y_1 or at its preimage $x_1^{(1)}$ (located at the steepest slope inflection points of $f_{\bar{\mu}_2}^{(4)}$ shown in Fig. 3). Once a trajectory is out of the cluster (contained between the maxima and minima of $f_{\bar{\mu}_2}^{(4)}$ next to the mentioned inflection points) it proceeds to the basin of attraction of an attractor phase (separated from the cluster by the inflection points with gentler slope of $f_{\bar{\mu}_2}^{(4)}$

in Fig. 3) where its final stage takes place. When considering a large ensemble of initial positions, distributed uniformly along all phase space, the common journey towards the attractor displays an exceedingly ordered pattern. Each initial position x_0 within either of the two clusters of sub-basins is a preimage of a given order k of a position in the main basin of attraction. Each iteration of $f_{\bar{\mu}_2}^{(4)}$ reduces the order of the preimage from k to $k-1$, and the new position $x'_0 = f_{\bar{\mu}_2}^{(4)}(x_0)$ replaces the initial position x_0 (a preimage of order $k-1$) of another trajectory that under the same time step has migrated to the initial position x''_0 (a preimage of order $k-2$) of another trajectory, and so on.

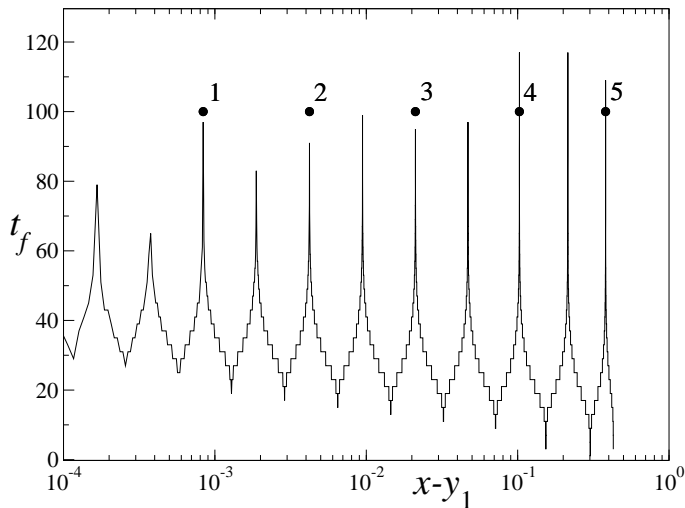


FIG. 11: Evolution of an orbit starting very close to a peak (repellor preimage) inside a cluster when $N = 2$, $\bar{\mu}_2 \simeq 1.31070264$ and $y_1 = 0.571663$. (See Fig. 4). The trajectory describes an exponential in time moving away from y_1 . In the figure, positions of the trajectory correspond to the black solid dots, and iterations correspond to the number associated to each dot.

It is clear that the dynamics at $\mu = \bar{\mu}_2$ displays sensitivity to the final state when the initial condition x_0 is located near the core of any of the two clusters of sub-basins at y_1 and $x_1^{(1)}$ that form the boundary of the attractor phases. Any uncertainty on the location of x_0 when arbitrarily close to these positions implies uncertainty about the final phase of a trajectory. There is also transient chaotic behavior associated to the migration of trajectories out of the cluster as a result of the organized preimage resettlement mentioned above. Indeed, the exponential disposition of repellor preimages shown in Fig. 5 is actually a realization of two trajectories with initial conditions in consecutive peaks of the cluster structure. Therefore, the exponential expression given in the previous Section in relation to Fig. 5 can be rewritten as the expression for a trajectory, $x_\tau \simeq x_0 \exp(\lambda_{eff}\tau)$, with, $x_\tau = x - y_1$, $x_0 = 7.5 \times 10^{-5}$, and $\lambda_{eff} = 6.4$, where $\tau = 1, 2, 3, \dots$. Straightforward differentiation of x_τ with respect to x_0 yields an exponential sensitivity to

initial conditions with positive effective Lyapunov coefficient λ_{eff} .

As it can be anticipated, the dynamics of approach to the next supercycle at $\mu = \bar{\mu}_3$ can be explained by enlarging the description presented above for $\mu = \bar{\mu}_2$ with the additional features of its preimage structure already detailed in the previous section. As in the previous case, trajectories with initial conditions x_0 located inside a cluster of sub-basins of the attractor phases will proceed to move out of it in the systematic manner described for the only two isolated clusters present when $\mu = \bar{\mu}_2$. Only now there is an infinite number of such clusters arranged into two bunches that group exponentially around the old repellor position y_1 and around its preimage $x_1^{(1)}$. See Figs. 6 to 8. Once such trajectories leave the cluster under consideration they enter into a neighboring cluster, and so forth, so that the trajectories advance out of these fractal boundaries through the prolonged process of migration out of the cluster of clusters before they proceed to the basins of the attraction of the eight phases of this cycle. In Fig. 12 we show one such trajectory in consecutive times $t = 1, 2, 3, \dots$ for the original map and also in multiples of time $t = 2^3, 2^3 \cdot 2^3, 3^3, \dots$. The logarithmic scale of the figure makes evident the retardation of each stage in the process. As when $\mu = \bar{\mu}_2$, it is clear that in the approach to the $\mu = \bar{\mu}_3$ attractor there is sensitivity to the final state and transitory chaotic sensitivity to initial conditions. Again, the exponential expression, given in the previous Section associated to the preimage structure of clusters of clusters of sub-basins shown in Fig. 7, can be interpreted as the expression of a trajectory of the form $x_\tau \simeq x_0 \exp(\lambda_{eff}\tau)$. Differentiation of x_τ with respect to x_0 yields again an exponential sensitivity to initial conditions with positive effective Lyapunov coefficient λ_{eff} .

When the period 2^N of the cycles increases we observe that the main characteristic in the dynamics is the development of a hierarchical organization in the flow of an ensemble of trajectories out of an increasingly more complex disposition of the preimages of the attractor phases. The role played by a cluster of sub-basins when $\mu = \bar{\mu}_2$ is preserved for the clusters present when $\mu = \bar{\mu}_3$ but the additional presence of clusters of clusters of sub-basins introduces a similar role in the dynamics at a broader scale in the preimage structure. A complication that will arise in a comparable fashion every time N increases.

IV. SUPER STRONG INSENSITIVITY TO INITIAL CONDITIONS

We turn now to discuss the closing point of the approach to the supercycle attractors and find out what is the form of the sensitivity to initial conditions ξ_t in the $t \gg 1$ limit, as required in its usual definition. The question is pertinent because for these attractors the ordinary Lyapunov exponent $\lambda \equiv \lim_{t \rightarrow \infty} t^{-1} \ln \left. \frac{df_{\bar{\mu}_N}^{(t)}(x)}{dx} \right|_{x=0}$

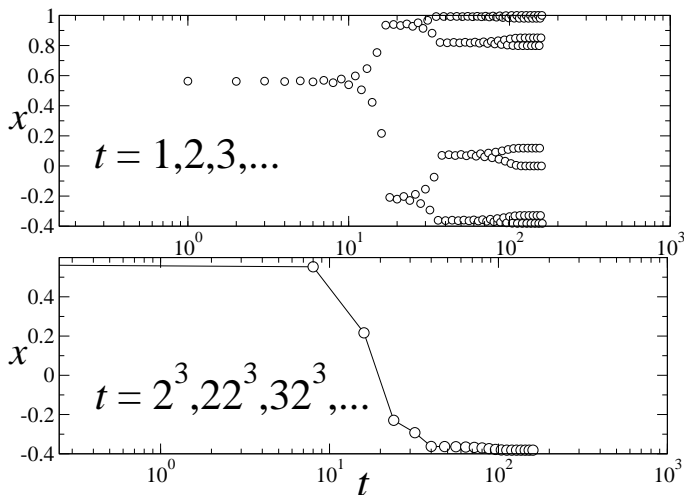


FIG. 12: A trajectory for $\bar{\mu}_3 \simeq 1.38154748$. Top panel: The circles are positions for consecutive times in the iterations of the map $f_{\bar{\mu}_3}(x)$. The orbit starts very close to the old (period one) repeller y_1 , then moves close to a period two and subsequently to a period four repeller, until finally the trajectory arrives at the period eight attractor. Bottom panel: Selection of a time subsequence of multiples of 2^3 shows the same trajectory as an evolution towards one particular attractor position.

diverges to minus infinity ($df_{\bar{\mu}_N}^{(t)}(x)/dx = 0$ at $x = 0$) and ξ_t cannot have an exponential form $\xi_t = \exp(\lambda t)$ with $\lambda < 0$.

Representative results for the last segment of a trajectory and the corresponding sensitivity ξ_t obtained from a numerical investigation are shown in Fig. 13. Only the first two steps of a trajectory with $x_0 = 0.1$ of the map $f_{\bar{\mu}_3}^{(2^3)}$ can be seen in Fig. 13 (a). A considerable enlargement of the spatial scale (that requires computations of extreme precision [9]) makes it possible to observe a total of seven steps (56 iterations in the original map), as shown with the help of logarithmic scales in Fig. 13 (b). Fig. 13 (c) shows both the same trajectory and the sensitivity $\xi_t \equiv dx_t/dx_0$ in a logarithmic scale for x_t and ξ_t and a normal scale for the time t . The trajectory is accurately reproduced (indistinguishable from the curve in Fig. 13 (c)) by the expression $x_t = u^{-1} \exp(b \exp ct)$, $b = \ln ux_0$ (with $x_0 > 0$) and $c = \ln 2$, where $u > 0$ is obtained from the form $|f_{\bar{\mu}_N}^{(2^N)}| \simeq ux^2$ that the 2^N -th composed map takes close to $x = 0$. This expression for x_t is just another form of writing $ux_t = (ux_0)^{2^t}$, the result of repeated iteration of ux^2 . For the logarithm of the sensitivity we have $\ln \xi_t = -\ln x_0 + t \ln 2 + \ln x_t$ where the last (large negative) term dominates the first two. Thus, we find that the sensitivity decreases faster than an exponential, and more precisely, decreases as the exponential of an exponential.

It is interesting to note that, associated to the general form $f_{\bar{\mu}_N}^{(2^N)}(x) \simeq ux^2$ of the map in the neigh-

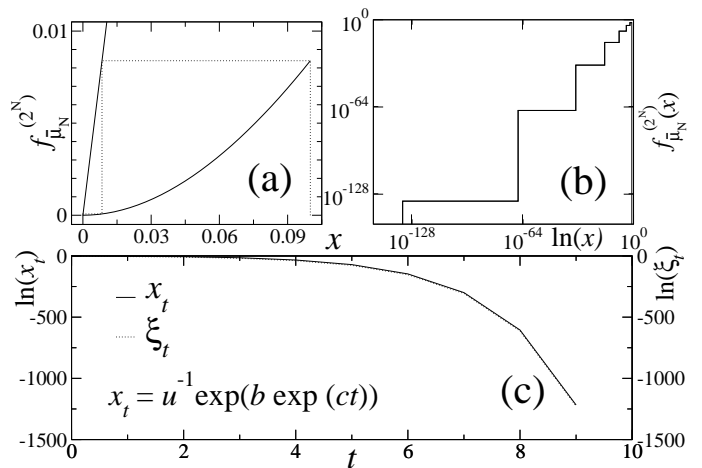


FIG. 13: Panel (a): Detail of a trajectory in its final stage of approach to the $x = 0$ attractor position (dotted line) for the map $f_{\bar{\mu}_3}^{(2^3)}(x)$ (solid line). In this example $N = 3$. Panel (b): Same as (a) in double logarithmic scale. Panel (c): Trajectory x_t and sensitivity to initial conditions ξ_t in logarithmic scale versus time t . Both functions are indistinguishable. Note that there is an ultra-rapid convergence, of only a few time steps, to the origin $x = 0$. See text.

borhood of $x = 0$, there is a map $f^*(x)$ that satisfies the functional composition and rescaling equation $f^*(f^*(x)) = \alpha^{-1} f^*(\alpha x)$ for some finite value of α and such that $f^*(x) = ux^2 + o(x^4)$. The fixed-point map $f^*(x)$ possesses properties common to all superstable attractors of unimodal maps with a quadratic extremum. Indeed, there is a closed form expression that satisfies these conditions. This is

$$f^*(x) = x \exp_q(u^{q-1}x),$$

where $\exp_q(x)$ is the q -exponential function $\exp_q(x) \equiv [1 + (1 - q)x]^{1/(1-q)}$. The fixed-point map equation is satisfied with $\alpha = 2^{1/(q-1)}$ and $q = 1/2$. The same type of RG solution has been previously found to exist for the tangent and pitchfork bifurcations of unimodal maps with general nonlinearity $z > 1$ [6], [4], [5]. Use of the map $f^*(x)$ reproduces the trajectory x_t/x_0 and sensibility ξ_t shown in Fig. 13 (c).

V. SUMMARY

We studied the properties of the first few members of the family of superstable attractors of unimodal maps with quadratic maximum and obtained a precise understanding of the complex labyrinthine dynamics that develops as their period 2^N increases. The study is based on the determination of the function $t_f(x_0)$, the time of flight for a trajectory with initial condition x_0 to reach the attractor or repeller. The novelty and scope of the study is that the function $t_f(x_0)$ was determined for *all* initial conditions x_0 in a partition of the total phase space

$-1 \leq x_0 \leq 1$, and this provides a complete picture for each attractor-repellor pair. We observed how the fractal features of the boundaries between the basins of attraction of the positions of the periodic orbits develop a structure with hierarchy, and how this in turn reflects on the properties of the trajectories. The set of trajectories produce an ordered flow towards the attractor or towards the repellor that reflect the ladder structure of the sub-basins that constitute the mentioned boundaries. As 2^N increases there is sensitivity to the final position for almost all x_0 , and there is a transient exponentially-increasing sensitivity to initial conditions for almost all x_0 . We observed that transient chaos is the manifestation of the trajectories' controlled flow out of the fractal boundaries, that suggest that for large 2^N the flow becomes an approximately self-similar sequence of stages. Finally, we looked at the closing segment of trajectories at which a very fast convergence to the attractor positions occurs. Here we found 'universality class' features, as the trajectories and sensitivity to initial conditions are replicated by an RG fixed-point map obtained under functional composition and rescaling. This map has the same q -deformed exponential closed form found to

hold also for the pitchfork and tangent bifurcations of unimodal maps [4], [5].

The new knowledge gained offers a significant qualitative and quantitative increment in the understanding of the dynamics at the transition to chaos, in this case via the period doubling route. The dynamics of approach to the Feigenbaum attractor and repellor, the supercycle of period 2^∞ , is, to our knowledge, not known at the level of detail given here for the first few supercycles. These comprehensive properties of the Feigenbaum attractor and repellor are presented [13] in tandem with this work. There is recent renewed interest in the dynamics of low-dimensional nonlinear maps as access to exact and detailed information for specific model systems is important in assessing theoretical developments, such as generalizations of ordinary statistics. There are positive indications that the multifractal critical attractors present in these maps play such role [10], [11], [12].

Acknowledgments. D.S. and A.R. are grateful to Hugo Hernández Saldaña for interesting discussions. Partial support by DGAPA-UNAM and CONACyT (Mexican Agencies) is acknowledged.

-
- [1] H.G. Schuster, *Deterministic Chaos. An Introduction*, 2nd Revised Edition, VCH Publishers, Weinheim, 1988.
- [2] C. Beck, F. Schlogl, *Thermodynamics of Chaotic Systems*, Cambridge University Press, UK, 1993.
- [3] R.C. Hilborn, *Chaos and Nonlinear Dynamics*, 2nd Revised Edition, Oxford University Press, New York, 2000.
- [4] A. Robledo, *Physica A* 314, 437 (2002); A. Robledo, *Physica D* 193, 153 (2004).
- [5] F. Baldovin, A. Robledo, *Europhys. Lett.* 60, 518 (2002).
- [6] B. Hu and J. Rudnick, *Phys. Rev. Lett.* 48, 1645 (1982).
- [7] C. Grebogi, S.W. McDonald, E. Ott, J.A. Yorke, *Phys. Lett.* 99A, 415 (1983).
- [8] S.W. McDonald, C. Grebogi, E. Ott, J.A. Yorke, *Physica* 17D, 125 (1985).
- [9] Our simulations used MAPM, the arbitrary precision C++ library (<http://www.tc.umn.edu/~ringx004/mapm-main.html>). We implemented our calculations taking between 200 and 1200 significant digits.
- [10] E. Mayoral, A. Robledo, *Phys. Rev. E* 72, 026209 (2005).
- [11] H. Hernández-Saldaña, A. Robledo, *Physica A* 370, 286 (2006).
- [12] A. Robledo, *Physica A* 370, 449 (2006).
- [13] A. Robledo, L.G. Moyano, *Phys. Rev. E* (submitted); /cond-mat/XXXX.